Ionogel-based hybrid polymer-paper handheld platform for nitrite and nitrate determination in water samples

Raquel Catalan-Carrio [a, b, 1], Janire Saez [b, c, *, 1], Luis Ángel Fernández Cuadrado [d], Gorka Arana [d], Lourdes Basabe-Desmonts [b, c, e, f, **], Fernando Benito-Lopez [a, e, f, ***]

[a] Microfluidics Cluster UPV/EHU, Analytical Microsystems & Materials for Lab-on-a-Chip (AMMa-LOAC) Group, Analytical Chemistry Department, University of the Basque Country UPV/EHU, Spain
[b] Microfluidics Cluster UPV/EHU, BIOMICs Microfluidics Group, Lascaray Research Center, University of the Basque Country UPV/EHU, Vitoria-Gasteiz, Spain
[c] Basque Foundation for Science, IKERBASQUE, Bilbao, Spain
[d] IBeA Group, Analytical Chemistry Department, University of the Basque Country UPV/EHU, Leioa, Spain
[e] Bioaraba Health Research Institute, Microfluidics Cluster UPV/EHU, Vitoria-Gasteiz, Spain
[f] BCMaterials, Basque Centre for Materials, Micro and Nanodevices, UPV/EHU Science Park, 48940, Leioa, Spain

HIGHLIGHTS

- Nitrite and nitrate detection into an ionogel matrix.
- Microfluidic PMMA and paper hybrid device.
- Multivariate statistical analysis by image analysis of real samples.
- Portable, easy to use and inexpensive device for environmental monitoring.

GRAPHICAL ABSTRACT
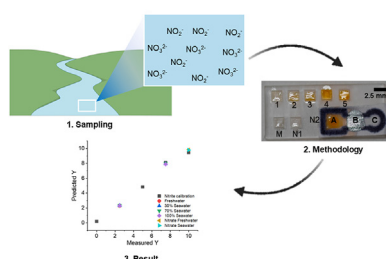
ARTICLE INFO

ABSTRACT

Nowadays, miniaturization and portability are crucial characteristics that need to be considered for the development of water monitoring systems. In particular, the use of handheld technology, including microfluidics, is exponentially expanding due to its versatility, reduction of reagents and minimization of waste, fast analysis times and portability. Here, a hybrid handheld miniaturized polymer platform with a paper-based microfluidic device was developed for the simultaneous detection of nitrite and nitrate in real samples from both, fresh and seawaters. The platform contains an ionogel-based colorimetric sensor for nitrite detection and a paper-based microfluidic device for the *in situ* conversion of nitrate to nitrite. The platform was fully characterized in terms of its viability as a portable, cheap and quick pollutant detector at the point of need. The calibration was carried out by multivariate analysis of the color of the sensing areas obtained from a taken picture of the device. The limits of detection and quantification, for

---

Paper microfluidics
Microfluidics

nitrite were 0.47 and 0.68 mg L^{-1}, while for nitrate were 2.3 and 3.4 mg L^{-1}, found to be within the limits allowed by the environmental authorities, for these two pollutants. Finally, the platform was validated with real water samples, demonstrating its potential to monitor nitrite and nitrate concentrations on-site as a first surveillance step before performing extensive analysis.

1. Introduction

Problems caused by environmental pollution are increasing social awareness, especially after the COVID-19 crisis when pollution levels decreased to historic minimums [1]. The inaccessibility to drinking water, due to human pollution, is causing massive animal and human migrations, diseases and deaths all over the world. Moreover, the pollution of water is triggering an irreparable loss of biodiversity and even threatening entire ecosystems. Therefore, it is imperative to monitor and then, control, water pollution levels to minimize environmental damages and guarantee proper access to potable water to the complete human population [2].

In this context, the world health organization (WHO) established methodologies principally based on reliable chromatographic and spectroscopic detection techniques [3], all of them requiring *in situ* sampling, followed by transport and storage of large sample volumes before pre-treatment of the sample and analysis at the laboratory facilities. These processes are generally slow and expensive to carry out. In the late 90's, researchers started to develop benchtop and portable instrumentation to make *in situ* analysis to eliminate transport and storage of the sample, minimizing its contamination [4–6]. In fact, in-field portable devices for the control of nitrite and nitrate are starting to be commercialized, offering good precision and accuracy, although device dimensions are still far from miniaturization [7], decreasing future applicability and commercialization. At this point, the intrinsic properties of microfluidics such as manipulation of small volumes, faster analysis times, better process control, small reagents consumption, reduced waste generation, compact device dimensions, and, in general, lower costs than conventional devices [8], make them very promising tools for environmental monitoring [9,10]. Different microfluidic devices have been developed for the detection of bacteria [11], heavy metals [12], emerging pollutants [13] and ions [14–17], helping to meet WHO specifications to improve the quality of life in developing countries [18], by providing easy and cheap devices for pollution evaluation and environmental analysis.

The development of microfluidic devices is, therefore, leading to the commercialization of easy to use kits for the analysis of parameters such as pH, nitrite, chloride or water hardness [19,20], which allows quicker analysis with a lower consumption of samples, increasing the frequency of analyses. As the WHO points out in their guidelines, these inexpensive, fast, and easy to use devices could be applied for non-formal screening, but usually, they do not satisfy the levels of precision compared to standardized methods [3]. Moreover, if these methods make use of smartphones, geolocation of the analyzed samples and instant communication of the results to the authorities are possible. Furthermore, these types of methodologies could be extended by using image analysis on smartphones for analyte detection. The detection of chlorine and nitrite [21], chemical oxygen demand, ammonia, nitrogen, and phosphate [22] are recently published examples. Additionally, the detection of heavy metals using image-assisted technologies, including smartphones [23], as well as the use of smartphones in paper-based microfluidic devices [24] has been recently reviewed, reinforcing the matching of image analysis with smartphones and microfluidics.

Nitrite and nitrate are natural components generated during the nitrogen cycle, but their presence in drinking water may lead to the eutrophication of waters; that is why, the WHO [3] and several environmental agencies [25,26] establish concentrations higher than 3 mg L^{-1} for nitrite, and 50 mg L^{-1} for nitrate as indicative of urban and/or industrial contamination.

Over the last century, the spectrophotometric assay based on the specific Griess reaction has been the most used method for the detection of both pollutants. This method involves a colorimetric diazo-coupling reaction between nitrite and the Griess reagent [27] where nitrite is directly detected. In addition, nitrate can also be detected, previous reduction to nitrite by using reducing agents, mainly Cd^0, but due to its toxicity it can be replaced by zinc (Zn^0) [28]. Since it is possible to precisely determine nitrite and nitrate concentrations in water samples via a simple colorimetric reaction, the use of portable microfluidic device instrumentation would reduce analysis costs, reagents consumption and waste generation, leading to Green Chemistry protocols [27,29,30]. Several microfluidic devices have been reported so far for the detection of nitrite and nitrate in water using electrochemical methods [30], but spectrophotometry [31] or color analysis [32,33] are the most widely used. In this context, it is worth highlighting those that make use of the Griess reaction both in paper [27,28,34–36] and poly(methyl)methacrylate (PMMA) [37,38] microfluidic devices. In many of the examples presented in the literature, the sensing of nitrite and nitrate was performed in solution by just adding a solution of the Griess reagent. Nevertheless, a major drawback of this approach is still the use of liquid reagents. Generally, the Griess reagent in solution, must be preloaded into containers or reservoirs outside the microfluidic device. Then, it is introduced into the device through pumps and valves, which considerably reduce the functionality of the device and its applicability at the point of need. Therefore, it would be desirable to have the sensing part within the microfluidic device in a solid substrate. For that purpose, ionogels (IOs) are good semi-solid matrixes due to their low vapor pressure, physical and chemical robustness and plasticizing capacity [39]. These matrixes may permit the Griess reaction to be performed within the gel and even to pre-concentrate the analytes, when water evaporates.

Our group has previously reported sensing molecules, integrated within microfluidic devices, based on ionogel (IO) materials, in a wearable format for the determination of pH [40] and lactate concentration [9] levels. Briefly, an IO is a hydrogel that contains an ionic liquid, maintaining the properties of ionic liquids, such as chemical and thermal stability, low vapor pressure, and high ionic conductivity in a gel semisolid structure. In 2016, we reported the first step on the development of a microfluidic device with an IO material, for the detection of nitrite and nitrate [41].

Here, we report a handheld miniaturized platform containing both the sample analysis and the calibration sites to perform the colorimetric detection of nitrite and nitrate in water samples using multivariate analysis of the color of the sensing sites, obtained from a taken picture of the device. The sensing sites are based on a new IO-based solid matrix assay able to change color in the presence of the analytes. Moreover, the platform incorporates a paper-based

device configuration, which allows the simultaneous detection of both analytes. The complete optimization of the platform and its analytical performance was carried out, eliminating the stability issues presented by previous configurations [41]. Finally, the platform was validated for the determination of nitrate and nitrite concentrations against conventional UV–Vis spectrophotometry. This platform represents the first portable handheld device based on an ionogel material with integrated Griess reaction for both nitrite and nitrate determination in real water samples.

2. Materials and methods

2.1. Fabrication of the handheld microfluidic platform

The handheld microfluidic platform was first designed in CorelDraw and fabricated using 1.1 mm thickness PMMA sheets purchased from Goodfellow (Huntingdon, UK). The fabrication of the different features of the platform was carried out using a CO_2 laser ablation system from Universal Laser Systems (Vienna, Austria).

The handheld microfluidic platform (32×15 mm) comprised four sections as shown in Fig. 1 (2. Methodology):

- (1–5) the calibration section with five reservoirs.
- (M) the matrix effect analysis section.
- (N1) the nitrite analysis section, to determine the nitrate concentration in the sample, all of the above with dimensions of 5×5 mm^2 and 0.5 mm depth.
- (N2) the nitrate analysis section, consisting of a paper-based (Whatman filter paper grade 595) microfluidic device with the IO matrix for the detection of the nitrate once reduced to nitrite.

The paper device was designed using AutoCAD™ and wax printed using a XEROX ColorQube 8580 with dimensions of 17×7 mm^2. A channel filled with Zn^0, deposited using a coating spray. The device was heated in a hotplate (Labnet International Inc., USA) for 6 min at 125 °C to form the hydrophobic walls, following the protocol published by our laboratory [42]. Next, a gasket made of four alternating layers of pressure sensitive adhesive (PSA) from Adhesive Research (Ireland) and cyclic olefin copolymer (COP) from Goodfellow (Huntingdon, UK), was added to deposit the IO solution and to avoid dispersion of the material

throughout the paper device before polymerization [43]. Immediately after deposition, the IO was polymerized for 10 min at 365 nm using a BONDwand UV-365 nm light source (Somerset, NJ, USA), washed three times with isopropanol (IPA) (EssentQ, Sharlab, Spain) and water, and left to dry for 24 h at room temperature.

The IO was synthesized following a similar protocol to the one previously described by us [44]. Briefly, 4.00 mmol of *N*-isopropylacrylamide monomer (NIPAMm), 0.08 mmol of *N, N′*-methylenebis(acrylamide) monomer (MBAAMm) as crosslinker and 0.04 mmol of 2,2-dimethoxy-2-phenylacetophenone (DMPA) as photoinitiator were dissolved in 1 mL of 1-ethyl-3-methylimidazolium dicyanamide ionic liquid all purchased from Sigma Aldrich (Madrid, Spain) and heated at 80 °C for 30 min with stirring. The preparation of the hydrogel for infrared analysis followed the protocol described above but the ionic liquid was substituted by Milli-Q water. Once the components were fully dissolved, the mixture was pipetted into the reservoirs (3 μL) and the gasket of the paper device mentioned before (6 μL) and photopolymerized. Then, the platforms were thoroughly washed three times with ultrapure water and isopropanol to eliminate the non-polymerized excess of ionic liquid, and were left to dry for 45 min before use while the paper device was left to dry for 24 h. The presence of the ionic liquid inside the ionogel and the comparison with the hydrogel, without ionic liquid, was investigated by Fourier-transform infrared spectroscopy (FTIR), in transmittance mode, using a Jasco 4200 spectrometer (Figure SI-1a).

The Griess reagent was prepared as a 1:1 mixture of sulphanilic acid (SAA) 1% in 5% of phosphoric acid 85% and *N*-1-naphtylethylendiamide dihydrochloride (NED) 0.1% in water, all acquired from Sigma-Aldrich (Madrid, Spain). The nitrate reduction to nitrite was done with Zn^0 spray, 98% purity, from Faren Chemical Industries (Madrid, Spain). All nitrite and nitrate standard solutions were prepared using sodium nitrate and sodium nitrite purchased from Sigma-Aldrich (Madrid, Spain). The presence of the Griess reagent inside the IO was evaluated by UV/Vis spectrophotometry and by scanning electron microscopy (SEM), Hitachi S- 4800 (Hitachi Japan). The presence of the Griess reagent in the IO changed the morphology of the polymer matrix from a swollen homogeneous to a globular microdomain structure (Figure SI-1b and c).

The pictures of the platforms with the X-rite ColorChecker Passport card (MSCCPP) (Grand rapids, MI, USA) were taken with a
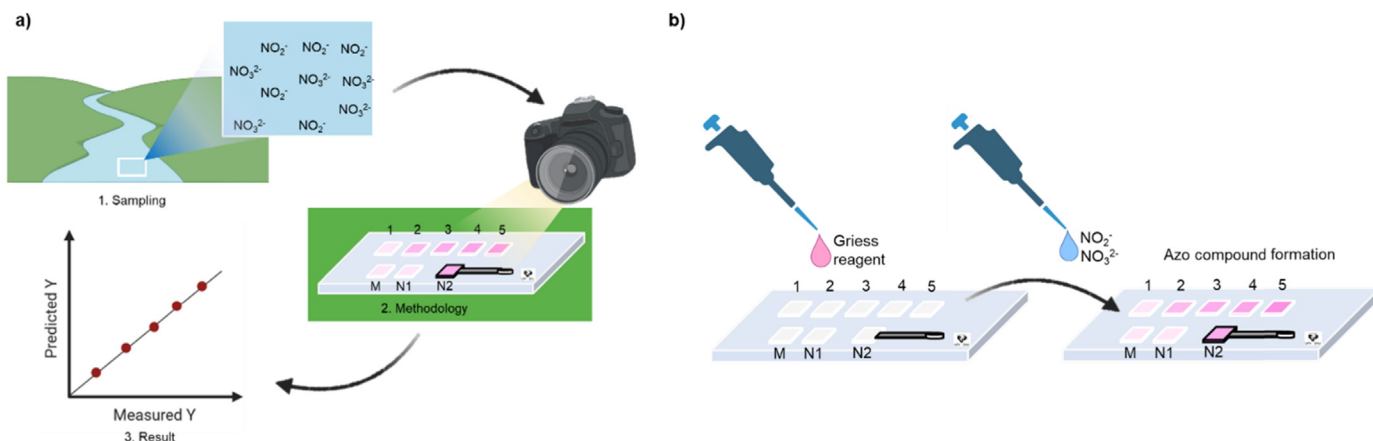

Fig. 1. a) Scheme of the complete analytical process developed in this work. 1) Freshwater samples containing the analytes. 2) Final device for the simultaneous detection of nitrate and nitrite and the set-up for taking the photos (simple camera). The oxidation process and color change of the azo compound to its nitro derivate by atmospheric oxygen occur in the IO reservoir of the device, over time. 3) Calibration using multivariate analysis of the color of the sensing sites, obtained from a taken picture of the device. b) Scheme of the working principle of the device. First, 3 μL (6 μL for the nitrate reduction system) of the Griess reagent are dropped into the inlets containing the ionogel matrix. Then, 3 μL (6 μL for the nitrate reduction system) of the water sample are dropped into the inlets containing the ionogel and the Griess assay. Finally, the purple color appears as a consequence of the Griess reaction. The color intensity varies with the concentration of nitrite in the sample. (For interpretation of the references to color in this figure legend, the reader is referred to the Web version of this article.)

Sony Cyber-Shot DSC-RX100 camera and analyzed as detailed in the detection protocol below, Figure SI-2.

2.2. Nitrite and nitrate color analysis detection protocol

For the calibration of nitrite, 3 μL of the Griess reagent solution were added and, once they got absorbed (120 s), five nitrite standard solutions of 0.0, 2.5, 5.0, 7.5 and 10.0 mg L^{-1} concentrations were prepared and pipetted on the five calibration reservoirs (1−5, respectively).

After 180 s, pictures of the device were taken and calibrated using an X-Rite ColorChecker Passport card (MSCCPP), with the Color-Checker Passport v.1.0.2 program, both from X-Rite Inc. (Grand rapids, MI, USA), placed beside the device over a neutral grey paper background to perform the camera calibration and assure the accuracy of the colors [45], See SI-Fig. 1a. The camera image plane was placed levelled in parallel to the plane of the device and the X-Rite Color Checker Passport and pictures were taken in RAW and JPG mode at once.

Then, the pictures were calibrated by using the CR_Calibrator_CC24 JavaScript Photoshop plug-in in Photoshop CC from Adobe Systems Inc. (Mountain view, CA, USA). The calibration of the pictures is necessary prior to any analysis, to assure the accuracy of the colors [46]. This plug-in opens the image multiple times, modifying the Photoshop color slides and selecting the settings that best fit all of them, in order to create a color calibration profile. Once the calibration was finished, the raw calibrated images were saved in JPG for further use. JPG format pictures were opened in the Photoshop CC program to estimate the representative chromaticity values (L, a* and b*) that were taken from centered points. 3 × 3 pixels areas were selected to obtain the points for each picture, avoiding shadows and reflection, determining their L, a* and b* values.

These values represent a three-dimensional color space model (CIELab color space) in Cartesian coordinates being L*, lightness, dark or light color, the black/white relation (0/100) and a* and b* the relationship between complementary colors or color wheel (hue), being neutral grey when a* and b* are 0. The red/green opposite colors are represented along the a* axis (green negative values and red positive values). The yellow/blue opponent colors are represented along the b* axis (blue negative values and yellow positive values) [47]. This type of color space is more suitable than the RGB model for analytical purposes because it has a wider color gamut, representing all the colors that the human eye is capable of detecting in a way that is independent of the device used, if calibrated as it is the case. However, for a quicker and simpler analysis, the RGB model would be enough to obtain the accuracy of colors.

Nowadays, the CIELCh system is becoming more popular among photographers since it was demonstrated being even more similar to how the human eye perceives color than CIELab [47,48]. Hence, the cylindrical coordinates C (chroma, saturated or dull color) and the h (angle of the hue in the CIELab model, color perceived) values were obtained from the L, a* and b* values by means of the following equations [48].

$$C = \sqrt{(a^2 - b^2)} \qquad \text{Eq. 1}$$

$$h = \tan^{-1}\frac{a}{b} \qquad \text{Eq. 2}$$

After obtaining the L, C and h values from the images, a Partial Least Squares (PLS) multivariate analysis was performed to evaluate the correlation between these variables and the concentration of nitrite. For that, The Unscrambler software (CAMO Analytics, Norway) was used [49].

Eight platforms were employed to obtain the nitrite calibration set (five for the calibration and three for the validation); the inlets of each platform were prepared with 3 μL of NaNO2 at different concentrations, ranging from 0 to 10 mg L^{-1}. Later, pictures of them were taken and the L, C, and h parameters were obtained. Subsequently, the PLS regression analysis with The Unscrambler software was performed. This regression was done considering L, C, and h as independent variables, while concentration remained as the dependent variable; besides, since a previous PCA analysis determined that only one principal component was able to explain the 97% of the variance [50] one principal component was used for the multivariate analysis.

During these experiments, it was observed that the purple color obtained from the Griess reaction changed over time to an orange/yellow color as depicted in Fig. 2. Consequently, a kinetic analysis of this change was done in order to establish the adequate waiting time before performing the analysis. Two devices were filled with the Griess reagent and nitrite solutions of 10 and 20 mg L^{-1}. Then, three pictures of each device were taken over 45 min, and the ratio between the Red and Blue colors, using a simpler RGB color space, was evaluated. When this ratio had a value of 1, the color obtained was purple (sum of red and blue) while as the Blue value decreased the color turned to orange/yellow, ratio >1.

2.3. Real sample analysis

Seawater samples were collected from the Plentzia marine station, Bizkaia (Spain) and aliquots with variable salinity of 30, 70 and 100% of seawater content in deionized water were prepared to study the influence of the ionic strength. Moreover, freshwater samples were collected from five selected points at Ullíbarri-Gamboa reservoir, Araba (Spain) (Figure SI-3). By using both types of samples, fresh and seawater, it was possible to evaluate the matrix effect and the recovery of the analyte in the device. For that, aliquots of both types of water samples were spiked with nitrite to reach a final concentration of 2.5, 7.5 mg L^{-1} and 100 mg L^{-1} of nitrate.

Moreover, two water samples from the Galindo (Bizkaia) water treatment plant, collected before and after the primary sedimentation process were filtered with a 0.45 μm pore size nylon filter, and analyzed as received, by both UV−Vis spectrometry (Shimadzu UV-1800, Japan) and the handheld platforms. Finally, the results of both methods were statistically compared to validate their performance.

3. Results and discussion

3.1. Reagent stability of the IO matrix

The storage stability of the IO matrix was investigated at different conditions; for that, two platforms with all their reservoirs filled with the IO matrix were employed. One of the platforms had all the IO reservoirs fulfilled with 3 μL of 5 mg L^{-1} of nitrite solution; while the other platform had all the reservoirs fulfilled with 3 μL of the Griess reagent. The behavior of both embedded IOs was investigated at two temperatures, 4 and 25 °C, in the darkness and in the darkness under vacuum conditions, to reduce the possible oxidation of the Griess reagent. Results showed that the IO with the embedded Griess reagent was stable up to 1 day, while the one with the nitrite solution was stable up to 3 days, independently of the conditions, as shown in Table 1. These results indicated that there was not a significant influence of the atmospheric oxygen and light conditions on the storage of the platforms.
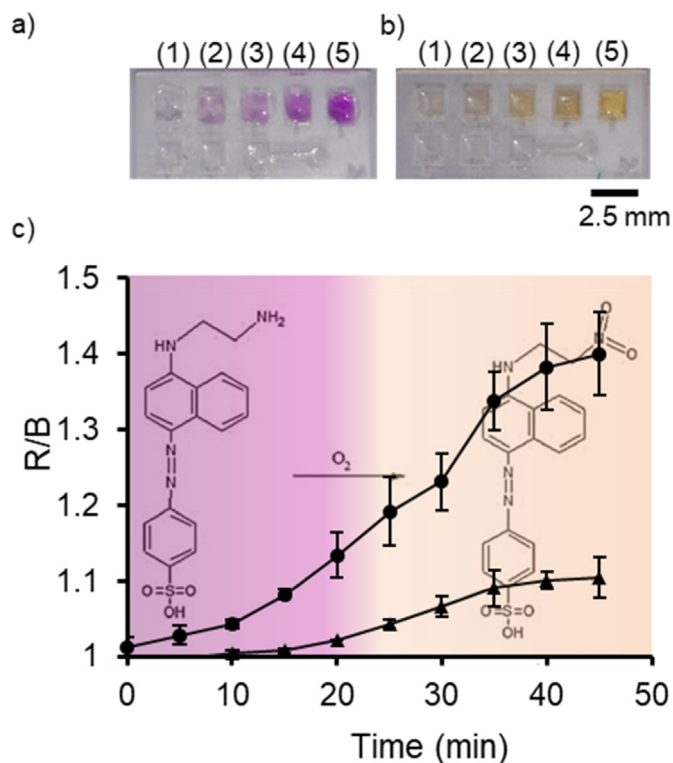
Fig. 2. a) Picture of the handheld platform with the on-site calibration section after 2 min and (b) after 40 min of the addition of the Griess reagent solution, being (1) 0.0, (2) 2.5, (3) 5, (4) 7.5 and (5) 10.0 mg L^{-1} of nitrite, respectively. c) Graph of the Red/Blue ratio during the oxidation process of the azo compound to its nitro derivate by atmospheric oxygen on the IO reservoir with a concentration of 10.0 (blue) and 20.0 mg L^{-1} (black) of nitrite, over time (n = 3). (For interpretation of the references to color in this figure legend, the reader is referred to the Web version of this article.)

3.2. Calibration optimization and multivariate analysis

The platform was designed as a single use device and envisioned as a set of reservoirs for on-site calibration, integrating all the necessary features to determine the nitrite and nitrate concentrations of water samples, as explained in detail in the Materials and Methods.

The linearity of the device in the range from 0.0 to 10.0 mg L^{-1} was investigated. For that, eight devices were fabricated, five of them were used to establish the calibration model and three to validate it. After the fabrication of the devices, the IO reservoirs of the calibration set were filled with the Griess reagent and then, the nitrite solutions, (1) 0.0, (2) 2.5, (3) 5.0, (4) 7.5 and (5) 10.0 mg L^{-1} were added to each of the IO reservoirs and an intense purple color immediately started to develop, as seen in Fig. 2a. Each reservoir

presented a characteristic purple tone, which increased in intensity with the nitrite concentration. However, after 3 min, this purple color started changing to an orange color due to the atmospheric oxidation of the azo compound (E)-4-((4-((2-aminoethyl)amino) naphthalen-1-yl)diazenyl)benzenesulfonic acid, formed during the Griess reaction, to (E)-4-((4-((2-nitroethyl)amino)naphthalen-1-yl) diazenyl)benzenesulfonic acid [51], Fig. 2b. Consequently, the kinetics of the oxidation process were studied using the Red/Blue ratio, to establish the optimum time in which the reaction was stable. This allowed getting the minimum time required to obtain a stable color (orange/yellow) on the device, 40 and 50 min for a nitrite concentration of 10.0 and 20.0 mg L^{-1}, respectively (Fig. 2c).

Additionally, further experiments performed to monitor color variations of the sensing material over time demonstrated that the orange/yellow color was stable at least for 3 days at room temperature and under standard diary laboratory light conditions (Figure SI-4). This shows that the IO introduces a matrix stable enough to perform the reaction and image analysis and, at the same time, allows storing the platform for further analysis, without needing any special storage protocols.

In order to obtain analytically relevant results from the handheld platform using the orange/yellow color calibration, a picture of the full platform, including the X-Rite ColorChecker Passport card, was taken, and the color of the sample was compared with the calibration. This calibration was done for the orange/yellow color after 40 min, to make sure that the color change is completed, Fig. 2b.

As it was previously mentioned, the calibration curve was obtained using a multivariate analysis in which first, the number of needed principal components was set as one [52] and then a PLS model was obtained for both the purple and orange colors (Fig. 3). The match between the theoretical and experimental values in the model indicated that the software is able to simulate the experimental colors obtained during the calibration process, allowing to create a prediction model to obtain the concentration of unknown samples from the L, C and h values. Furthermore, as the results obtained by different platforms, in different moments and at uncontrolled environmental conditions, were indistinguishabled, thus it can be considered that the obtained results were reproducible.

In consequence, according to the stability of the orange/yellow color and the stability of the IO matrix, the platform could be used with the calibration part already done up to 24 h after the addition of the Griess reagent solution to the sample reservoirs (N1 and N2). This could be an advantage since in the standardized spectrophotometric methods, the Griess reagent has to be always freshprepared prior to analysis. Therefore, the handheld platforms could be used for on-site analyses of unknown nitrite concentrations at the point of interest, e.g. in field, since it would be just necessary to pipette the water samples in the reservoirs and wait

Table 1
Study of the influence of time, temperature, light, and atmospheric oxygen during the storage of the handheld device with the reagent solutions embedded in the IO reservoirs, up to 5 days.

Environment conditions							
IO fulfilled with	25 °C light	25 °C light, vac.	25 °C darkness, vac.	4 °C light	4 °C light, vac,	4 °C darkness, vac.	Days
Nitrite	✓	✓	✓	✓	✓	✓	1
	✓	✓	✓	✓	✓	✓	3
	✗	✗	✗	✗	✗	✗	5
Griess reagent	✓	✓	✓	✓	✓	✓	1
	✗	✗	✗	✗	✗	✗	3
	✗	✗	✗	✗	✗	✗	5

Where ✓ indicates that the device was operative and ✗ indicates that the device was not operative after storage. Three devices were used for each experiment obtaining the same results.
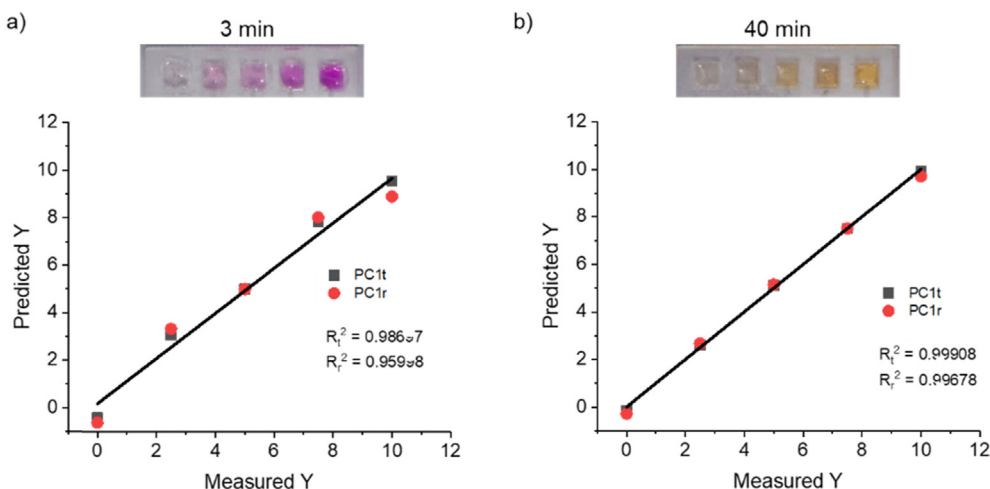
Fig. 3. Multivariate regression for the calibration of the reaction of the Griess reagent with nitrite at different concentrations, using PLS. a) Pictures were taken 3 min after the addition of the Griess reagent to the IO reservoirs. b) Pictures were taken 40 min after the addition of the Griess reagent to the IO reservoirs. At that time, the orange/yellow colour was stable. Theoretical NO_2^- values (PC1t) are depicted in dark grey and experimental NO_2^- values (PC1r) are depicted in red (n = 5). (For interpretation of the references to color in this figure legend, the reader is referred to the Web version of this article.)

for 40 min to obtain the result. It is worth mentioning at this point that the purple color obtained during the first minutes could be also used to obtain a qualitative estimation of the nitrite concentrations, when compared with the image of the calibrations taken from the 1−5 calibration area of the handheld platform. Thus, these tones could be registered in a picture and later compared with the purple tone of the sample to obtain a pseudo-quantitative analysis or even done by just direct eye observation. The portability could be improved by the incorporation of blisters in the device that act as reservoirs of the Griess reagent to eliminate the need for pipetting; nevertheless, the stability of the reagent solution would need to be investigated in the blister too.

3.3. Optimization of nitrate analysis with the handheld platform

As explained in detail in the Materials and Methods section, the nitrate detection has a paper-based microfluidic device with Zn^0 immobilized on it to reduce the nitrate from the sample to nitrite. In order to do that, the water sample containing both nitrate and nitrite was pipetted in the circular reservoir of the device. Then, the solution was forced to pass through the paper-based microfluidic device containing Zn^0 by capillary forces. Along its trajectory, the nitrate was reduced to nitrite when getting in contact with the Zn^0, immobilized on the paper substrate. Finally, the solution reached the IO of the nitrite analysis reservoir, where the Griess reagent reacted with all the nitrite present in the solution and changed the color of the IO. The color was then analyzed by image analysis using the protocol mentioned before, and the concentration of nitrate was determined by subtracting the value obtained in the reservoir N2 (Fig. 4a), the one obtained in reservoir N1.

The performance of section N2 of the handheld device was investigated by pipetting in the inlet of the paper-based microfluidic device with a known concentration of nitrate, 50 mg L^{-1}. The solution was left for 10 min to react, by passing through the channel with Zn^0. Then, a solution of the Griess reagent was pipetted on the IO and the color formation, due to the presence of nitrite was investigated after 15 min, as explained in the Materials and Methods section. Eight replicates of this device were used to investigate the conversion of nitrate to nitrite, obtaining a nitrite concentration of 10.1 ± 0.6 mg L^{-1}. Thus, taking into account that we pipetted a concentration of nitrate of 50 mg L^{-1}, our paper-based reactor was able to perform the reduction from nitrate to nitrite with a 20 ± 1% conversion efficiency. This conversion yield could be improved, if necessary, by increasing the Zn^0 microchannel length to allow longer reaction times.

3.4. Limits of detection and quantification of the method

In order to obtain the limits of detection (LOD) and quantification (LOQ) of this platform, it is necessary to go through their definitions by the International Union of Pure and Applied Chemistry (IUPAC).

$$Limit = s_{blank} + k\,\sigma^2 \hspace{2cm} \text{Eq. 3}$$

where s_{blank} is the blank signal, consisting of an IO reservoir filled with deionized water and Griess reagent solution, σ^2 is the standard deviation of the blank signal and k is a constant value that depends on the limit studied: $k = 3$ for the limit of detection (LOD), and $k = 10$ for the limit of quantification (LOQ). Therefore, a LOD of 0.47 mg L^{-1} and a LOQ of 0.68 mg L^{-1} were obtained for nitrite, as can be seen in Table 2.

The LOD and LOQ for nitrate, considering the 20% efficiency of the reduction to nitrite in the paper microfluidic device, were calculated to be 2.3 and 3.4 mg L^{-1}, respectively. These detection limits are two orders of magnitude higher than those reached by the spectrophotometric methods currently used in water analysis. However, they are good enough to satisfy the limits demanded by health and environmental agencies, opening a real possibility to introduce portable microfluidic platforms to screen in field, sampling points and to decide if it would be necessary or not to carry out a more in depth analysis of a certain sample.

3.5. Determination of nitrite and nitrate concentrations in real water samples

Fresh and seawater samples were used to study the ionic strength and matrix effect of the handheld platform. Ionic strength studies were performed by using different seawater samples spiked with nitrite (2.5 and 7.5 mg L^{-1}) at different seawater percentages (30, 70 and 100% seawater in deionized water). On the other hand, freshwater samples, spiked with the same nitrite solutions, were
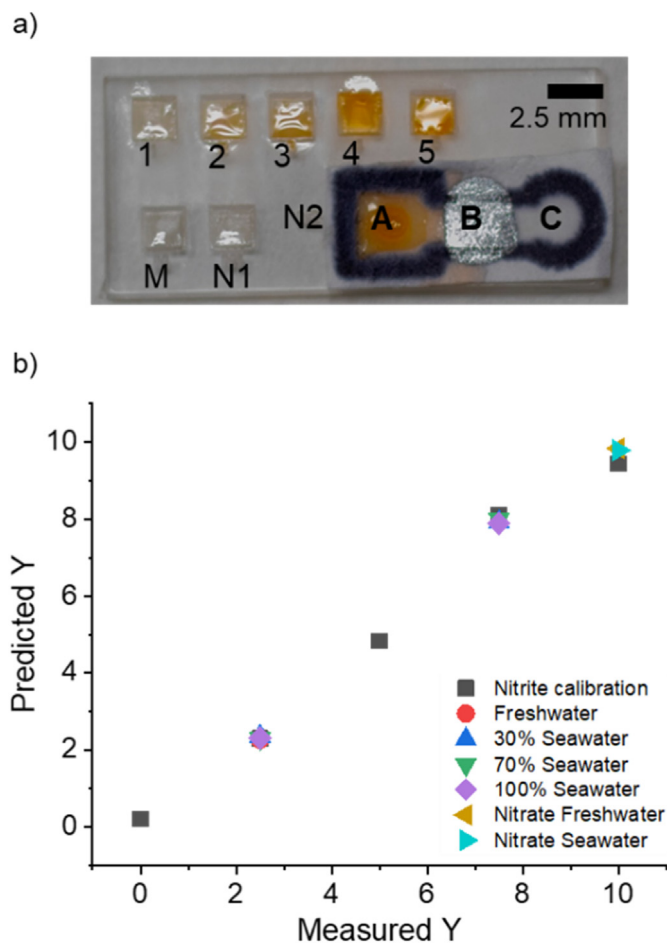
Fig. 4. a) Picture of the IO-based hybrid polymer-paper handheld platform after the addition of the Griess reagent and sample solutions, 40 min (1–5) calibration section, (M) matrix analysis section, (N1) nitrite analysis sample section (N2) nitrate analysis section. N2 contains the paper-based microfluidic device: (A) nitrite analysis reservoir, (B) microfluidic channel with deposited Zn^0, (C) inlet for sample addition. b) Multivariate regression for the calibration of the reaction of Griess reagent with nitrite at different concentrations, using PLS with the results obtained for the samples of spiked nitrite (2.5, 7.5 and 100.0 mg L^{-1}). The samples employed freshwater and 30, 70 and 100% of seawater as matrixes.

Table 2
Blank signal values and predicted concentration of nitrite by The Unscrambler program to calculate the LOD for nitrite.

Parameters			Predicted concentrations (mg L^{-1})
L	C	h	
73.70	7.00	85.60	0.35
69.70	8.00	90.00	0.38
70.00	8.57	90.50	0.41

used to study the possible matrix effect (see Materials and Methods). The accuracy between the colors obtained and those obtained for the standards (Fig. 4b) was studied, and no significant differences were observed, showing the robustness of the matrix against ionic strength variations, and the recovery of the analyte and absence of matrix effect. Fig. 4b shows the calibration by PLS and the comparison with the values obtained for the 30, 70 and 100% of seawater samples and the freshwater samples, spiked with 2.5 and 7.5 mg L^{-1} of nitrite, showing that the Griess reaction was not influenced by either the seawater or the freshwater. Thus, it can be concluded that the colorimetric response of the handheld

platform is not affected by the water matrixes investigated and, therefore, it can be used for the analysis of both sea and freshwater samples.

The validation was done by comparing the results obtained using the platform with those obtained by using UV−Vis spectrophotometry on two samples from a Wastewater Treatment Plant in Galindo (Bizkaia, Spain). For the UV−Vis analysis (see the Materials and Methods section), concentrations of nitrite of 0.85 ± 0.07 and 0.42 ± 0.07 mg L^{-1} (n = 3) were obtained for the two samples, respectively. At the same time, six handheld devices, using a total amount of 18 μL of the sample were used to obtain a concentration of nitrite of 0.77 ± 0.06 and 0.30 ± 0.07 mg L^{-1} (n = 6), respectively. The validation of the handheld platform was studied by comparing the results obtained for both methods using the *F* and *t* statistical tests, and it was found out that the variances of the methods were different, while the average values could be considered comparable within a 95% confidence level. This indicated that even though the precision was different, the nitrite concentrations obtained using both methods were the same and, with this, the results obtained by our device could be considered reliable and validated against a standardized method.

The delivered device has demonstrated its potential to be used to monitor nitrite and nitrate concentrations on-site as a first surveillance step before performing extensive analysis. The next step will focus on the development and integration of a smartphone app that will perform the colorimetric analysis, sample points geolocation, and remote storage of the data.

4. Conclusions

The fabrication and performance of a handheld miniaturized polymer platform with a paper-based microfluidic device capable of detecting nitrite and nitrate concentrations in real water samples by colorimetric detection were presented. The analytical parameters for the colorimetric detection of nitrate and nitrite water samples were studied by analyzing the L, C and *h* parameters from images of the platform. The LOD and LOQ of the device for both nitrite and nitrate were obtained resulting in a LOD for nitrite of 0.47 mg L^{-1}, which is below the maximum value permitted for national and international water regulations (3 mg L^{-1}), despite being higher than those for standardized methods. In the case of nitrate, although the percentage of conversion was low (20 ± 1%) a LOD of 2.3 mg L^{-1} was obtained, which is also below the values from official regulatory entities (50 mg L^{-1}). Qualitative information can be obtained in just 3 min, by comparing the purple color obtained with a reference picture of the calibration. After that, quantitative analysis can be performed in only 15 min, after complete formation of the orange/yellow color.

The stability of the IO matrix permits the use of the handheld device up to 24 h after its fabrication, incorporating the complete calibration set, and the Griess reagent into the sample reservoirs. Therefore, the calibration could be done in advance; and in this way, the device could be used at the point of need since just the sample needs to be added, followed by a photograph of the platform after 40 min. Furthermore, no matrix effect was found to interfere with the colorimetric analysis, and the performance of the platform was not influenced by the ionic strength, which been consequently useful for nitrate and nitrite determination in both, fresh and seawater. Finally, the performance of the platform was validated by comparing the performance of the device with a standardized UV−Vis spectrophotometry, obtaining that both methods gave the same concentration of nitrite when analyzing real water samples.

The low volumes of both, reagents and samples, needed for the analysis are a great saving for the fabrication and the mass

production of these types of devices, which also implies a lower generation of waste. Additionally, the use of image analysis assures that detection can be adapted to a smartphone configuration, whose software could directly analyze the data to generate an even more user-friendly detection methodology.

Funding sources

Author Contributions

The manuscript was written through contributions of all authors. / All authors have given approval to the final version of the manuscript.

CRediT authorship contribution statement

Raquel Catalan-Carrio: Methodology, write and correct the manuscript, Writing − original draft. **Janire Saez:** Design, write and correct the manuscript, Writing − original draft. **Luis Ángel Fernández Cuadrado:** Methodology, correct the manuscript. **Gorka Arana:** Methodology, correct the manuscript. **Lourdes Basabe-Desmonts:** Correct the manuscript, Supervision, the manuscript, Funding acquisition. **Fernando Benito-Lopez:** Design, write, correct and supervision the manuscript, Writing − original draft, Funding acquisition.

Declaration of competing interest

The authors declare that they have no known competing financial interests or personal relationships that could have appeared to influence the work reported in this paper.

Acknowledgments

Appendix A. Supplementary data

Supplementary data to this article can be found online at https://doi.org/10.1016/j.aca.2022.339753.

References

[1] S. Rousseau, N. Deschacht, Environ. Resour. Econ. 76 (2020) 1149−1159.
[2] P. Gleick, Water Int. 21 (1996) 83−92.
[3] J.A. Cotruvo, J. AWWA (Am. Water Works Assoc.) (2017) 44−51.
[4] E.T. Steimle, E.A. Kaltenbacher, R.H. Byrne, Mar. Chem. 77 (2002) 255−262.
[5] A. Tzoris, D. Fearnside, M. Lovell, E.A.H. Hall, Environ. Toxicol. 13 (2002) 284−290.
[6] G.M. Greenway, S.J. Haswell, P.H. Petsul, Anal. Chim. Acta 387 (1999) 1−10.
[7] Aquamonitrix Ltd. https://aquamonitrix.com/. Last accessed Oct 2021.
[8] S.A. Jaywant, K.M. Arif, Sensors 19 (2019) 4781.
[9] D. Khodagholy, V.F. Curto, K.J. Fraser, M. Gurfinkel, R. Byrne, D. Diamond, G.G. Malliaras, F. Benito-Lopez, R.M. Owens, J. Mater. Chem. 22 (2012) 4440−4443.
[10] M. Czugala, R. Gorkin, T. Phelan, J. Gaughran, V.F. Curto, J. Ducrée, D. Diamond, F. Benito-Lopez, Lab Chip (2012) 5069−5078.
[11] N. Yamaguchi, Y. Fujii, Biol. Pharmaceut. Bull. 43 (2020) 87−92.
[12] S. Cinti, V. Mazzaracchio, G. Öztürk, D. Moscone, F. Arduini, Anal. Chim. Acta 1029 (2018) 1−7.
[13] A.L. Campaña, S.L. Florez, M.J. Noguera, O.P. Fuentes, P. Ruiz Puentes, J.C. Cruz, J.F. Osma, Biosensors 9 (2019) 41.
[14] P. Cao, Y. Zhu, W. Zhao, S. Liu, H. Gao, Water 11 (2019) 2339.
[15] J.J. Peters, M.I.G.S. Almeida, L. O'Connor Šraj, I.D. McKelvie, S.D. Kolev, Anal. Chim. Acta 1079 (2019) 120−128.
[16] M. Fiedoruk-Pogrebniak, M. Granica, R. Koncki, Talanta 178 (2018) 31−36.
[17] H. Nawaz, J. Zhang, W. Tian, K. Jin, R. Jia, T. Yang, J. Zhang, J. Hazard Mater. 387 (2020) 121719.
[18] A. St John, C. Price, Clin. Biochem. Rev. 3 (2014) 155−167.
[19] A.D. Beaton, V.J. Sieben, C.F.A. Floquet, E.M. Waugh, S. Abi Kaed Bey, I.R.G. Ogilvie, M.C. Mowlem, H. Morgan, Sensor. Actuator. B Chem. 156 (2011) 1009−1014.
[20] K.Y. Castillo-Torres, E.S. McLamore, D.P. Arnold, Micromachines 11 (2019) 16.
[21] M. Sargazi, M. Kaykhaii, Spectrochim. Acta Mol. Biomol. Spectrosc. 227 (2020) 117672.
[22] H. Jiang, B. Sun, Y. Jin, J. Feng, H. Zhu, L. Wang, S. Zhang, Z. Yang, ACS Sens. 5 (2020) 3013−3018.
[23] R. Jain, A. Thakur, P. Kaur, K. Kim, P. Devi, Trac. Trends Anal. Chem. 123 (2020) 115758.
[24] C. Carrell, A. Kava, M. Nguyen, R. Menger, Z. Munshi, Z. Call, M. Nussbaum, C. Henry, Microelectron. Eng. 206 (2019) 45−54.
[25] Official Journal of the European Communities, European Commission 75/440/EEC, 1975.
[26] Quality Criteria for Water, EEUU Environmental Protection Agency EPA 440/5-86-001, 1986.
[27] T.M.G. Cardoso, P.T. Garcia, W.K.T. Coltro, Anal. Methods 7 (2015) 7311−7317.
[28] L. Merino, Food Anal. Method 2 (2009) 212−220.
[29] Y. Xiong, C. Wang, T. Tao, M. Duan, S. Fang, M. Zheng, Anal. Bioanal. Chem. 408 (2016) 3413−3423.
[30] X. Wang, M.R. Gartia, J. Jiang, T. Chang, J. Qian, Y. Liu, X. Liu, G.L. Liu, Sensor. Actuator. B Chem. 209 (2015) 677−685.
[31] M.F. Khanfar, W. Al-Faqheri, A. Al-Halhouli, Sensors 17 (2017) 2345.
[32] H. Hwang, Y. Kim, J. Cho, J. Lee, M. Choi, Y. Cho, Anal. Chem. 85 (2013) 2954−2960.
[33] E. Murray, P. Roche, K. Harrington, M. McCaul, B. Moore, A. Morrin, D. Diamond, B. Paull, J. Chromatogr. A 1603 (2019) 8−14.
[34] D. Gabriel, J. Baeza, F. Valero, J. Lafuente, Anal. Chim. Acta 359 (1998) 173−183.
[35] Y. Kiso, Y. Jung, K. Kuzawa, Y. Seko, Y. Saito, T. Yamada, M. Nagai, Chemosphere 64 (2006) 1949−1954.
[36] B.M. Jayawardane, S. Wei, I.D. McKelvie, S.D. Kolev, Anal. Chem. 86 (2014) 7274−7279.
[37] M. Czugala, C. Fay, N.E. O'Connor, B. Corcoran, F. Benito-Lopez, D. Diamond, Talanta 116 (2013) 997−1004.
[38] T.L. Mako, A.M. Levenson, M. Levine, ACS Sens. 5 (2020) 1207−1215.
[39] A. Kavanagh, R. Byrne, D. Diamond, K.J. Fraser, Membranes 2 (2012) 16−39.
[40] V.F. Curto, C. Fay, S. Coyle, R. Byrne, C. O'Toole, C. Barry, S. Hughes, N. Moyna, D. Diamond, F. Benito-Lopez, Sensor. Actuator. B Chem. 171−172 (2012) 1327−1334.
[41] J. Saez, G. Arana, L.A. Fernandez-Cuadrado, F. Benito-Lopez, Procedia Eng. 168 (2016) 518−521.
[42] R. Catalan-Carrio, T. Akyazi, L. Basabe-Desmonts, F. Benito-Lopez, Sensors 21 (2020) 101−113.
[43] T. Akyazi, N. Gil-González, L. Basabe-Desmonts, E. Castaño, M.C. Morant-Miñana, F. Benito-Lopez, Sensor. Actuator. B Chem. 247 (2017) 114−123.
[44] T. Akyazi, J. Saez, J. Elizalde, F. Benito-Lopez, Sensor. Actuator. B Chem. 233 (2016) 402−408.
[45] O. Liñero, M. Cidad, G. Arana, C. Nguyen, A. de Diego, Microchem. J. 134 (2017) 284−288.
[46] H. Yu, T. Cao, B. Li, R. Dong, H. Zhou, 3rd International Conference on Information Science and Control Engineering, ICISCE, 2016.
[47] R. Korifi, Y. Le Dréau, R. Antinelli, R. Valls, N. Dupuy, Talanta 104 (2013) 58−66.
[48] W. Swasty, J. Sosioteknologi 17 (2018) 171−176.
[49] A.S. Camo Software, The Unscrambler User Manual, 2006.
[50] M. Shariati-Rad, M. Irandoust, M. Haghighi, Int. J. Environ. Sci. Technol. 12 (2015) 3837−3842.
[51] J.B. Fox, Anal. Chem. 51 (1979) 1493−1502.
[52] M.O. Salles, G.N. Meloni, W.R. de Araujo, T.R.L.C. Paixao, Anal. Methods 6 (2014) 2047−2052.